

An Efficient and Error-Resilient Protocol for Quantum Random Access Memory with Generalized Data Size

Zhao-Yun Chen,^{1,*} Cheng Xue,¹ Tai-Ping Sun,^{2,3,4} Huan-Yu Liu,^{2,3,4} Xi-Ning Zhuang,^{2,5}
Meng-Han Dou,⁵ Tian-Rui Zou,⁵ Yuan Fang,⁵ Yu-Chun Wu,^{1,2,3,4,†} and Guo-Ping Guo^{1,2,3,4,5,‡}

¹*Institute of Artificial Intelligence, Hefei Comprehensive National Science Center, Hefei, Anhui, 230026, P. R. China*

²*CAS Key Laboratory of Quantum Information, University of Science and Technology of China, Hefei, Anhui, 230026, P. R. China*

³*CAS Center For Excellence in Quantum Information and Quantum Physics, University of Science and Technology of China, Hefei, Anhui, 230026, P. R. China*

⁴*Hefei National Laboratory, Hefei, Anhui, 230088, P. R. China*

⁵*Origin Quantum Computing Company Limited, Hefei, Anhui, 230026, P. R. China*
(Dated: March 10, 2023)

Quantum Random Access Memory (QRAM) is a critical component for loading classical data into quantum computers. However, constructing a practical QRAM presents several challenges, including the impracticality of an infinitely large QRAM size and a fully error-correction implementation. In this work, we address the challenge of word length, as real-world datasets typically have larger word lengths than the single-bit data that most previous studies have focused on. We propose a novel protocol for loading data with larger word length k without increasing the number of QRAM levels n . By exploiting the parallelism in the data query process, our protocol achieves a time complexity of $O(n+k)$ and improves error scaling performance compared to existing approaches. We also provide a data-loading method for general-sized data access tasks when the number of data items exceeds 2^n , which outperforms the existing hybrid QRAM+QROM architecture. Our protocol contributes to the development of time and error-optimized data access protocols for QRAM devices, reducing the qubit count and error requirements for QRAM implementation, and making it easier to construct practical QRAM devices with physical qubits.

I. INTRODUCTION

Quantum computing has experienced rapid growth in recent years, with the potential to solve problems that classical computers cannot efficiently solve [1–3], and to improve performance on computationally expensive classical tasks such as quantum machine learning [4–6] and quantum differential equation solvers [7–10]. However, a significant challenge in quantum computing is the classical data loading task. In order to process real-world data with quantum algorithms, the quantum states must first be prepared from classical data [11, 12]. If 2^n data entries are encoded in the quantum circuit, the gate complexity is at least $O(2^n)$, which may negate any potential quantum speedup if the encoding procedure is also $O(2^n)$. This difficulty is discussed in detail in [13]. Because this task is essential for many quantum algorithms, Quantum Random Access Memory (QRAM) was introduced to address this problem [14–20].

QRAM, a quantum analog of classical Random Access Memory (RAM), can efficiently load classical data into a quantum computer and allows querying in quantum superposition. The QRAM achieves its efficiency by exploiting circuit-level parallelism, using $O(2^n)$ an-

cillary qubits to load $O(2^n)$ data items with $O(n)$ time complexity. The exponential qubit count required for implementing a scalable QRAM has been one of the most challenging aspects, as even a small error rate in qubits can lead to large errors in the entire system. To overcome this issue, a promising QRAM architecture called the bucket-brigade architecture was proposed in [15] which has already been demonstrated to be error-resilient [21].

While practical applications of QRAM are desirable, several challenges must be addressed. The first challenge is the inherent difficulty in implementing the bucket-brigade QRAM architecture with fault tolerance. It requires an exponential number of qubits and non-Clifford gates[21], which cannot be transversally encoded in any quantum error correction codes[22–24]. For instance, a single query from a surface-code-based QRAM would require an exponential number of T gates, making the required number of magic states intractable[25]. A promising approach to achieve a practical application of the QRAM is to build it with high-quality physical qubits and error suppression methods such as error filtration[26] to further reduce errors. As a result, QRAM must operate with a limited number of qubits and cope with noisy qubits without any error correction.

A further challenge in implementing QRAM is the issue of word length. Prior research has mainly focused on the case where each data entry is a single bit, and an exact n -level QRAM is used to route each of the 2^n bits independently. However, in real-world applications, data

* chenzhaoyun@iaai.ustc.edu.cn

† wuyuchun@ustc.edu.cn

‡ gpguo@ustc.edu.cn

entries are usually composed of multiple bits, which are referred to as the “word length” in classical computing. If we denote the word length as k , then we need to load $2^n k$ bits in total. Addressing this more general task is essential for practical QRAM implementation. One can increase the number of QRAM levels to $n + \log k$ to address each bit uniquely, or increase the bandwidth or query sequentially to handle the generalized data loading task (as mentioned in [17, 21]). However, these approaches have significant drawbacks, such as the need to build at least k -fold qubits and/or having a k -fold error rate, which severely challenges the practicality of QRAM.

Here, we aim to improve the performance of the generalized data-loading task with limited resources and noisy qubits. To achieve this, we propose a QRAM protocol based on the bucket-brigade architecture, named the “parallel protocol.” Our protocol achieves $O(n + k)$ time complexity for querying 2^n k -bit data items with an n -level bandwidth-1 QRAM, without the need to increase the number of levels or the bandwidth. This time complexity is a significant improvement over previous works. Furthermore, it is also possible for the number of data entries to exceed 2^n . We generalize the parallel protocol for querying 2^{m+n} k -bit data with n -level QRAM and achieve $O(n + 2^m k)$ time complexity. More importantly, our protocol shows an optimal error scaling of the same task with n -level QRAM, even when the bandwidth of the QRAM is increased. As a result, this protocol reduces the requirements for building a QRAM for practical usage in quantum algorithms, and it is a promising step toward developing efficient quantum algorithms that can handle large-scale classical data.

This paper is organized as follows. In Section II, we first introduce the fundamentals of the bucket-brigade QRAM with arbitrary word length, the qubit-based and qutrit-based schemes, and the data loading task. We then present the design of our parallel protocol, including the fundamental operations and the query process. Section III provides a comparison of our protocol’s performance with other possible methods that implement the same tasks, including time complexity, qubit number, and error. In Section IV, we conduct a numerical simulation to evaluate our protocol’s error performance and compare it with another protocol. Section V discusses the generalization of our parallel protocol to arbitrary-sized data-loading tasks and introduces the hybrid-parallel protocol. Finally, in Section VI, we conclude our results and outlook for the future challenges of the QRAM.

II. PARALLEL PROTOCOL OF THE BUCKET-BRIGADE QRAM

A. Preliminaries

Firstly, we present our definition of the data-loading task with arbitrary word length.

Definition 1 (QRAM with arbitrary word length). *An (n, k) -QRAM acts on two quantum registers $|i\rangle_A$ and $|z\rangle_D$, where register A has n qubits and D has k qubits, stores exactly 2^n entries of k -bit classical data d_i ($i \in [0, 2^n - 1]$), and implements U_{QRAM} such that*

$$U_{\text{QRAM}}|i\rangle_A|z\rangle_D = |i\rangle_A|z \oplus d_i\rangle_D. \quad (1)$$

The (n, k) -QRAM determines the address length n and word length k , which respectively represent the size of the address and data register, with each classical data entry also being a k -bit string. It is important to note that this study focuses on the bucket-brigade QRAM architecture by default. Other alternatives, such as the fanout architecture or QROM, have an error scaling that grows exponentially with the input size, especially with the address size n [21]. Therefore, considering that the QRAM is sensitive to errors, we do not consider them suitable candidates for a scalable QRAM architecture. Additionally, we have noticed a quantum walk-based QRAM architecture[17, 18], which will be further discussed in Section III.

Figure 1 depicts a possible design of a quantum computer, consisting of a quantum processing unit (QPU) and a bucket-brigade QRAM. They are connected by an address bus and a data bus, which correspond to the QRAM’s input registers A and D for the unitary U_{QRAM} , respectively. The bucket-brigade QRAM is structured by a binary tree that connects the bus with the classical memory nodes, and tree nodes are composed of qudits (including qubit, qutrit, or more levels). A conceptual diagram of the structure is shown in Fig. 1(b). In the following text, we will mark each node by a pair of integers (l, p) , where l denotes layer number and p represents the position in the layer where $0 \leq p \leq 2^n - 1$. For example, the root node is $(0, 0)$, and its left and right children are marked as $(1, 0)$ and $(1, 1)$ correspondingly.

Each node in the binary tree contains two qudits: an address qudit A and a data qudit D . Generally, the address qudit marks the address route, while the data qudit transfers bits along the route. We classify the architecture into two schemes based on the type of qudit used for the address register: qutrit-based or qubit-based. As illustrated in Fig. 1(c), the qubit-based scheme uses a qutrit for A and a qubit for D , while the qutrit-based scheme employs qubits for both A and D . We propose this classification because the two schemes have different error scales. The number of levels for the data qudit determines the number of bits that can be transferred at a time, namely the bandwidth of the QRAM. For simplicity, the data qudit is set to be one qubit (bandwidth-1), and the higher-bandwidth case will be discussed later on.

The QRAM query process involves three stages: address setting, data fetch, and uncomputing. During the address setting stage, a path is established from the root of the tree to the bottom, corresponding to the address of the data entry being queried. In the data copy stage, the data is first transferred from the data bus register to the tree root, then to the memory nodes to retrieve the data

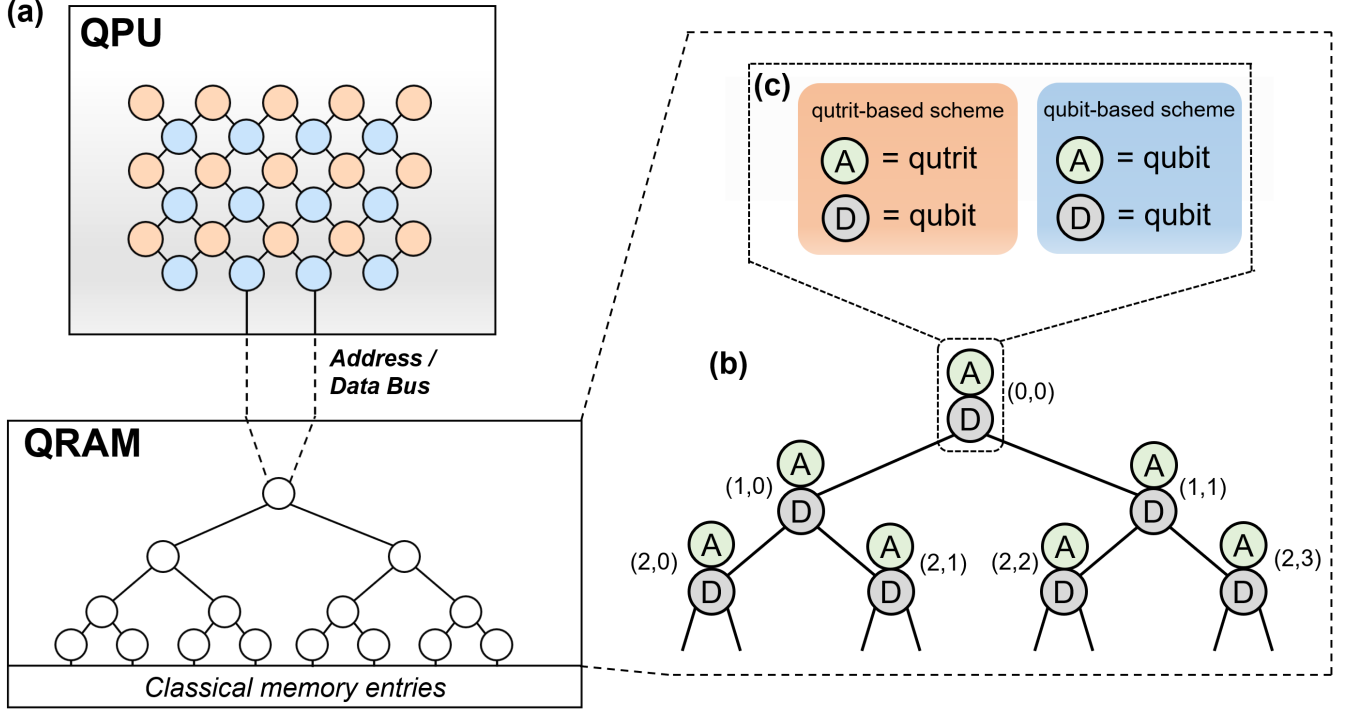


FIG. 1: (a) Schematic of possible quantum computer architecture that includes a quantum processing unit (QPU) and a quantum random access memory (QRAM). The QPU connects the QRAM with a bus that transfers the address and the data state to the root of the QRAM. With a binary tree, QRAM connects with a classical memory. (b) The structure of the bucket-brigade QRAM. The structure is a full binary tree of n layers. Each tree node is marked by a pair of integers, where the first denotes the number of the layer, the second the position within the layer. (c) The tree node has two cases in our protocol: a qutrit-based scheme and a qubit-based scheme. The qutrit-based scheme consists of an address qutrit and a data qubit. In the qubit-based scheme, the address qutrit is replaced by a qubit. The bottom of the tree is the classical memory. Each of the classical memory contains k bits.

bit, and finally returned to the bus. In the uncomputing stage, the address setting stage is reversed to return the system to its initial state. Note that the QRAM should be implemented unitarily, which is often considered a default requirement in many algorithms, such as those that involve reflection operations or uncomputation [27, 28]. This requirement allows the QRAM to not only map $|i\rangle|0\rangle$ to $|i\rangle|d_i\rangle$, but also to perform the inversion. Therefore, it is important to completely uncompute all side effects that occur during the query process to ensure that the state of the QRAM is fully restored, with changes only to the state of the buses.

B. Fundamental operations

This section introduces the fundamental operations involved in QRAM queries in the quantum circuit model, which provides a clear way to model the time sequence and error. Figure 2 depicts the circuit for all operations, which include two versions for qutrit and qubit-based schemes, respectively. In the following, the three levels of a qutrit are denoted by $|L\rangle$, $|R\rangle$, and $|W\rangle$, while the

states of a qubit are denoted by $|0\rangle$ and $|1\rangle$. The state of A in node (l, p) is denoted by $|a^{l,p}\rangle$, and the state of D is denoted by $|d^{l,p}\rangle$. The state of the i -th qubit in the address and data bus is represented by $|A_i\rangle$ and $|D_i\rangle$, respectively. Finally, m_n denotes the n -th classical memory bit.

The *Routing* operation swaps the data qubit of a node with one of its children according to the state of the address qutrit, which is illustrated in Fig 2(a) and (d). In the qutrit-based scheme, it is

$$R_t = |W\rangle\langle W| \otimes I + |L\rangle\langle L| \otimes \text{SWAP}^L + |R\rangle\langle R| \otimes \text{SWAP}^R. \quad (2)$$

And in the qubit-based scheme, it is

$$R_b = |0\rangle\langle 0| \otimes \text{SWAP}^L + |1\rangle\langle 1| \otimes \text{SWAP}^R. \quad (3)$$

The *internal swap* operation exchanges the data between $a^{(l,p)}$ and $d^{(l,p)}$. In the qubit-based scheme, the internal swap simply consists of two swap operations on the address qubit and data qubit, which is illustrated in Fig. 2(e). But in the qutrit-based scheme, it is conditioned by the activeness of the parent node. Fig. 2(b) is an example. The internal swap is only necessary when the connections between qutrits are limited and there only

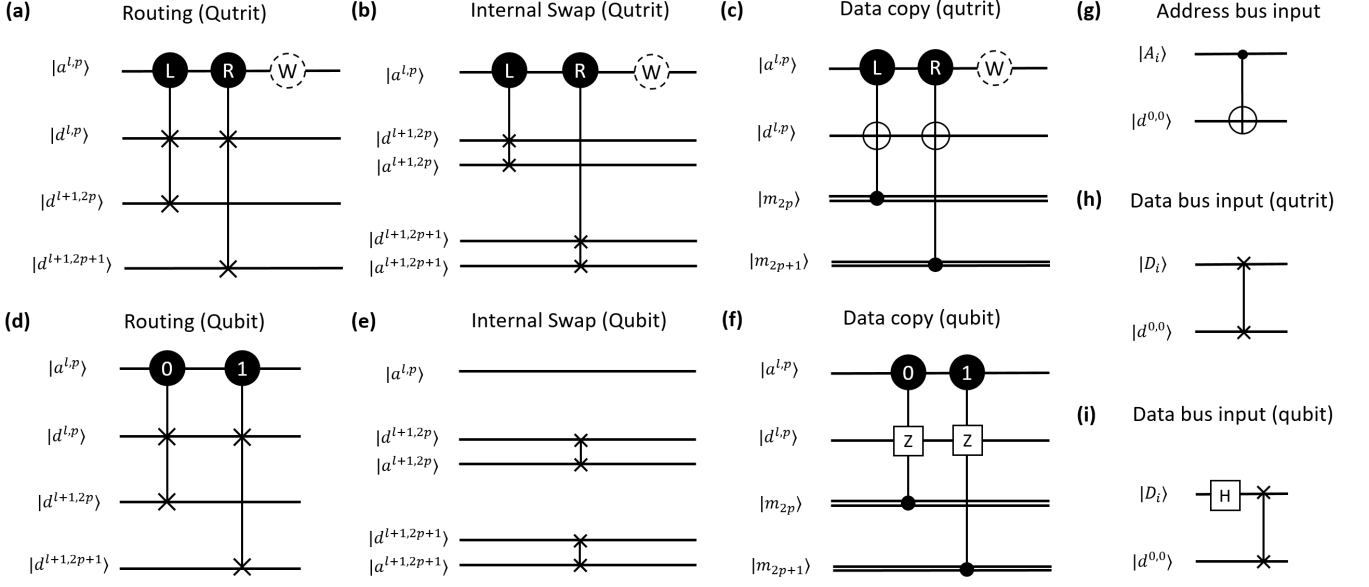


FIG. 2: The fundamental operations in QRAM, denoted by quantum circuit model. (a) Routing operation in the qutrit scheme. (b) Internal swap in the qutrit scheme. Note that this operation is also controlled by the activeness of the parent node. (c) Data copy, denoted by M_i in the qutrit model. (d)(e)(f) Same as (a), (b), and (c), but in the qubit-based scheme. (g) The address bus input operation, which copies the address bus into the tree root. Note that this operation is identical in both schemes. (h) The data bus input operation in the qutrit-based scheme, which moves the data bus into the tree root. (i) Same as (h), but in the qubit-based scheme.

allow routing operations between data qubits. If the connection is more flexible, one can directly apply the routing operation on the children nodes' address qubits instead of data qubits. Note that the internal swap operations are filled in the interval between other operations, and whether the connection has such a limitation will not affect the time sequence.

The *data copy* operation fetches the classical data to the data qubit by a classical controlled operation, shown in Fig. 2(c) and (f). In the qutrit-based scheme, this is a classical-controlled controlled-not operation and in the qubit-based scheme, this is a controlled-Z operation where the data is encoded by the phase of the data qubit.

The *address bus input* shares the same circuit in both schemes. It copies the i -th digit of the address bus to the root node using a CNOT operation. This input circuit will also be applied when in the uncomputing stage.

The *data bus input* for the qutrit-based scheme is to move the i -th digit from the data bus to the root node using a swap operation. Not copying the data bus but moving it allows the uncomputing of the QRAM operation in the quantum algorithms. In the qubit-based scheme, we should apply a Hadamard on the data bus first and encode the bit on the phase of the qubit.

Routing, *internal swap*, and *data copy* operations can form into layered operations, which means that we will simultaneously apply this operation to an entire layer. For example, a layered *routing* R_t^l is applied on all nodes in layer l . This parallelism is fundamental for the logarithm

time scaling of the QRAM.

C. Process of the parallel protocol

In this section, we introduce our QRAM protocol that implements an (n, k) -QRAM. We call this protocol the *parallel protocol* because the main optimization comes from the parallelism achieved in the three stages of the QRAM process. This parallelism arises because we do not need to process each bit one by one. Instead, we can begin to process each address bit or data bit before its predecessor reaches its target. For instance, before an address qubit reaches its corresponding layer, another qubit can already enter the tree because the former route has already been carved. Moreover, different data qubits will not affect each other, even if their paths collide as one is entering and another is exiting the tree. With this principle, we are able to construct an operation sequence in which we only have to apply the *address bus input* and then *data bus input* operations compactly to push every input bus qubit into the tree.

We will now provide a detailed description of each stage of our QRAM protocol. The first stage is the address setting stage, where each digit of the address is pushed sequentially to a different level of the binary tree. Parallelism is achieved as each digit follows the path carved by its predecessors, and the next digits can be pushed in before the current digit reaches its destina-

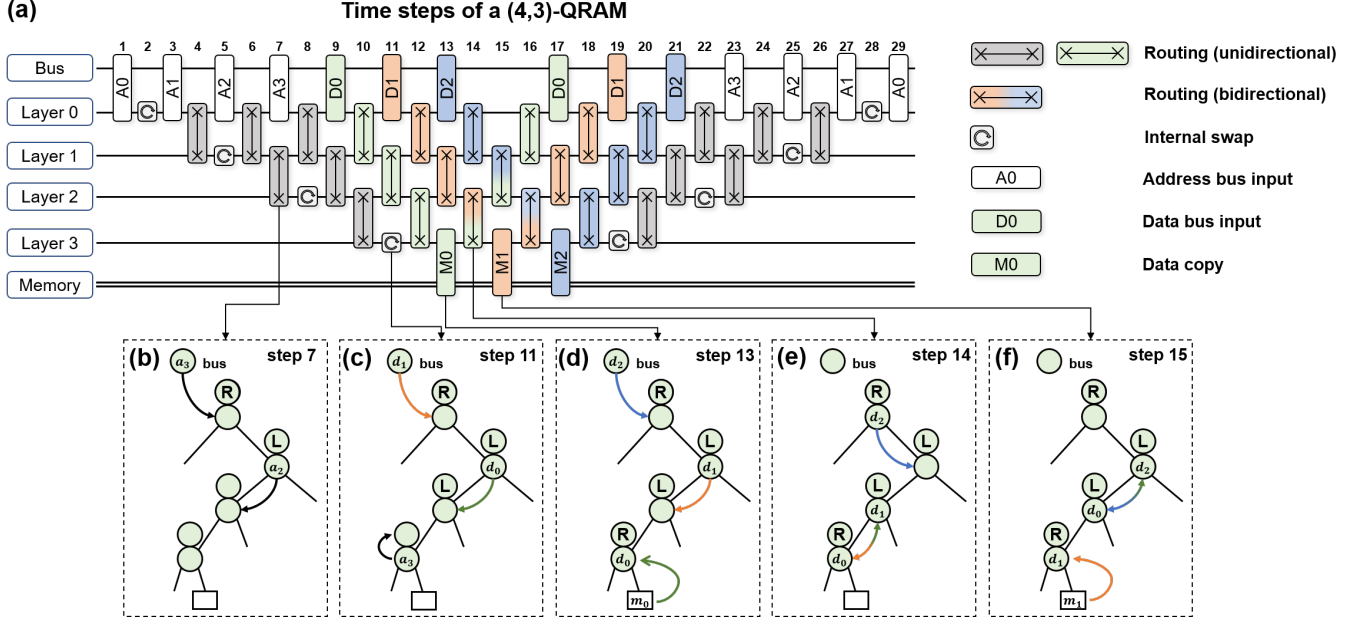


FIG. 3: An example for the quantum circuit representation of a (4, 3)-QRAM. (a) The time steps of a (4,3)-QRAM. Each horizontal line corresponds to a layer of the structure including the bus, QRAM, and memory. The legend of icons is shown on the right. Each icon can be a layered operation if the corresponding layers have more than one target. We mark the route of the three data bits with green, red, and blue colors. When two data bits are swapped in the neighbor layer (two routes collide), we use the gradient color to mark the bidirectional routing. (b) (f) The behaviors of the data movement in five typical time steps of the branch with address 1001. Each circle represents a qudit, and each tree node consists of two qudits. The upper circle is the address qubit/qutrit, and the lower is the data qubit. The arrow denotes the movement of a bit.

tion.

In the data fetch stage, each digit of the data bus travels from the root to the leaves, performs the classical controlled operation, and then travels inversely. Similar to the address setting stage, the digit can enter the tree after the last digit has moved to the next layer, which reduces the number of time steps required. Each data bit follows a zig-zag route, first moving downwards and then upwards, forming a folded trajectory that may intersect with the path of another data bit. When two routes collide, one routing operation is bidirectional, which allows for both upwards and downwards movement at the same time. As a result, after the address setting stage is completed, one can retrieve data from the memory through the same path without having to repeatedly set the address. When the word length is k , one only needs to repeat the data fetch k times.

As an example, the quantum circuit representation of a (4,3)-QRAM is shown in Fig 3(a). In this representation, each wire represents all nodes in its layer, and the quantum operations (including routing, internal swap, and data copy) are layered operations that are executed simultaneously on all nodes in their layers. To make the movement of each data digit clear, different colors are used to distinguish the route taken by each data bit.

The digit transition process is illustrated through five typical time steps from (b) to (f) in Fig 3(a). The address

setting stage demonstrates its parallelism starting from step 7, where A3 enters the tree and A2 moves from layer 1 to layer 2 simultaneously. Similarly, in the data fetch stage, step 13 (shown in (d)) allows D0, D1, and D2 to move simultaneously. Steps 14 and 15 (shown in (e) and (f) respectively) demonstrate the parallelism of the data fetch stage. In time steps 14 and 15, the collision of two color bands illustrates how a single operation enables the simultaneous upward and downward movement of two data digits. It is worth noting that this circuit representation applies to both the qutrit-based and qubit-based schemes, with each module set to its corresponding version.

III. PERFORMANCE COMPARED WITH OTHER PROTOCOLS

In this section, we will show the performance of the parallel protocol and compare it with other possible implementations of the (n, k) -QRAM, including the qubit number, the time complexity, and the error scaling. There are two trivial ideas for extending $(n, 1)$ -QRAM to (n, k) -QRAM. One is using the nonparallel version where each bit is queried sequentially, where we name it *nonparallel protocol*. Another is extending the data qubit to multiple qubits (e.g. m -qubit) in each tree node,

TABLE I: Performance of the different protocols.

Protocol Name	Qubit number	Time complexity	Error scaling (qutrit-based)	Error scaling (qubit-based)	Cost factor (qutrit-based) $T\epsilon_t/n\epsilon$
Parallel (this paper)	$O(2^n)$	$O(n+k)$	$O((n+k)n\epsilon)$	$O((n+k)n^2\epsilon)$	$(n+k)^2$
Nonparallel	$O(2^n)$	$O(nk)$	$O(kn^2\epsilon)$	$O(kn^3\epsilon)$	k^2n^2
High-bandwidth	$O(c2^n)$	$O(nk/c)$	$O(kn^2\epsilon)$	$O(kn^3\epsilon)$	k^2n^2/c
Quantum-walk based[17]	$O(n+k)$	$O(n\log(n+k))$	-	-	-

namely extending the bandwidth, where we name it *high-bandwidth protocol*. In Fig 4, we illustrate the conceptual diagram for the execution processes of these protocols. The horizontal bands represent the QRAM layers, and the slant lines represent the movement of the data. First, we present an intuitive summary of the comparison of the performance of the different protocols in Table I. Then, we will discuss them in detail and make a comparison.

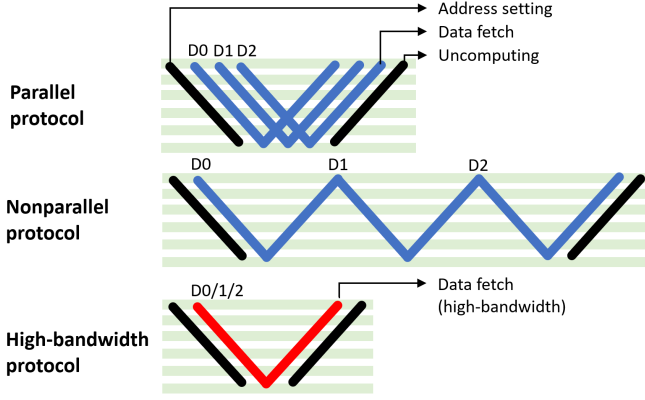


FIG. 4: The schematic diagram for the execution processes of different protocols. Horizontal bands represent the QRAM layers, and the slant from left to right represents the time sequence of data movement. The black slant represents the address setting stage or the uncomputing stage. The blue slant represents the data fetch stage of bandwidth one. The red slant is the high-bandwidth data fetch stage, where more than one digit of data can be transferred in a batch.

A. Time complexity and qubit number

The time complexity of the parallel protocol for the (n, k) -QRAM is given below.

Proposition 1 (Time complexity of the parallel protocol). *The time complexity of the (n, k) -QRAM is $O(n+k)$ in the qutrit-based scheme and qubit-based scheme where n is the address size, k the data size.*

For the parallel protocol, adding one more data qubit will only increase the number of time steps by 2, as the last data qubit has just left the tree root when the new

data qubit enters the tree. Therefore, the time complexity of our protocol is linear in both n and k , resulting in an overall time complexity of $O(n+k)$.

For the nonparallel protocol, the address setting stage takes the same $2n$ time steps. The data fetch stage has k sequential data qubit's process, where the number of the time step is $2nk$. The uncomputing stage is the same as the address setting stage. The total number of time steps is $2nk + 4n$, and the asymptotic complexity is $O(nk)$. In the high-bandwidth protocol with bandwidth c , a data qutrit is constructed by c qubits. Therefore, in the data fetch stage, we can allow it to transfer k data bits in k/c batches and obtain the time complexity $O(nk/c)$.

The time complexity of the parallel protocol shows a substantial speedup over the nonparallel protocol. Note that this complexity is asymptotically optimal with $O(2^n)$ qubits, as the limited bandwidth contributes at least $O(k)$, and the time for addressing each data bit is at least $O(n)$.

The qubit number of the parallel protocol and the nonparallel protocol is independent of the data length k , and the space complexity (qubit number) is $O(2^n)$, which is proportional to the number of the tree nodes of n layers. The high-bandwidth protocol, as we have mentioned earlier, has c qubits for the data qutrits, so the qubit number is $O(c2^n)$.

B. Error scaling

Despite the qubit number and the time complexity, the parallel protocol mainly optimizes the error scaling of the QRAM.

Proposition 2 (Error scaling of the parallel protocol). *The fidelity of the (n, k) -QRAM is F_1 in the qutrit-based scheme and F_2 in the qubit-based scheme. We have $F_1 \geq 1 - O((n+k)n\epsilon)$ and $F_2 \geq 1 - O((n+k)n^2\epsilon)$, where ϵ is the error rate of each qutrit and is sufficiently small.*

The proof of the error scaling mainly inherits the idea in [21]. To calculate the error scaling, one has to determine the fraction of *good branches*, which $\Lambda = 1 - nT\epsilon$ where T is the execution time and ϵ is the error rate for each qubit. Then we have the error scaling as $1 - (2\Lambda - 1)^2 = O(nT\epsilon)$. The error scaling consists of two components: the error rate of each node throughout the entire process, which is $O(T\epsilon)$, and the average number of branches affected by a single node's error.

To extend the proof from $(n,1)$ -QRAM to (n,k) -QRAM, we only need to change the execution time in the proof from n to $n+k$ (for the parallel protocol) or nk (for the nonparallel protocol). For the high-bandwidth protocol with bandwidth c , the error rate for a single node is replaced by $O(c\epsilon)$. A detailed description of this extension is provided in Appendix Section A.

The results show that the parallel protocol preserves the error resilience, where the word length k appends an extra $O(kn\epsilon)$ error to the system and it finally has $O((n+k)n\epsilon)$ and $O((n+k)n^2\epsilon)$ error scaling in the qutrit-based scheme and qubit-based scheme, correspondingly. In contrast, the nonparallel has $O(kn^2\epsilon)$ error in the qutrit-based scheme and $O(kn^3\epsilon)$ in qubit-based, which increases the amount of error by a factor of k . Similarly, the high-bandwidth protocol increases the error of each qubit from ϵ to $c\epsilon$. Our results demonstrate that our proposed protocol is highly efficient for building a QRAM with generalized input size. For a typical case where $n = k = 32$, the error rate is improved from $O(n^3)$ to $O(n^2)$ and resulting in an approximately 16-fold improvement.

The error filtration method, which can suppress error in a black box unitary, is promising to be used to reduce the error of QRAM if we cannot achieve a fault-tolerant[26]. Using error filtration, we can apply T noisy black box unitary with ϵ error to achieve the same unitary but with ϵ/T error. With this technique, we can define the cost factor of the QRAM by $T\epsilon_t/n\epsilon$, where ϵ_t is the total error scaling and ϵ the error of a single qubit, shown in Table I. A lower cost factor represents better performance. Apparently, the parallel protocol is better than the nonparallel protocol and a high-bandwidth protocol for any $k > 1$.

C. Comparison with the quantum-walk-based architecture

Recently, a quantum-walk-based QRAM architecture has been proposed[17, 18]. This architecture also considered the case where the word length is more than 1. In the proposal, an (n,k) -QRAM can be implemented using $n+k$ quantum walkers on a directed graph, which uses $O(n+k)$ qubits and achieves $O(n \log(n+k))$ time complexity.

The scaling of the qubit number and time does not mean it does not consume exponential resources. Instead, a quantum walker is like a “flying qubit” and can travel coherently through quantum switches. Therefore, the number of quantum switches and the circuit width is exponential to the address length.

The time complexity of the quantum-walk QRAM is $O(n \log(n+k))$. Intuitively, when k is a constant (such as $k = 1$), an $O(n \log n)$ is already a slow-down over the bucket-brigade architecture, which is $O(n)$; also, the quantum-walk QRAM has a speedup when k is sufficiently larger than 1 to let $n+k > n \log(n+k)$. While

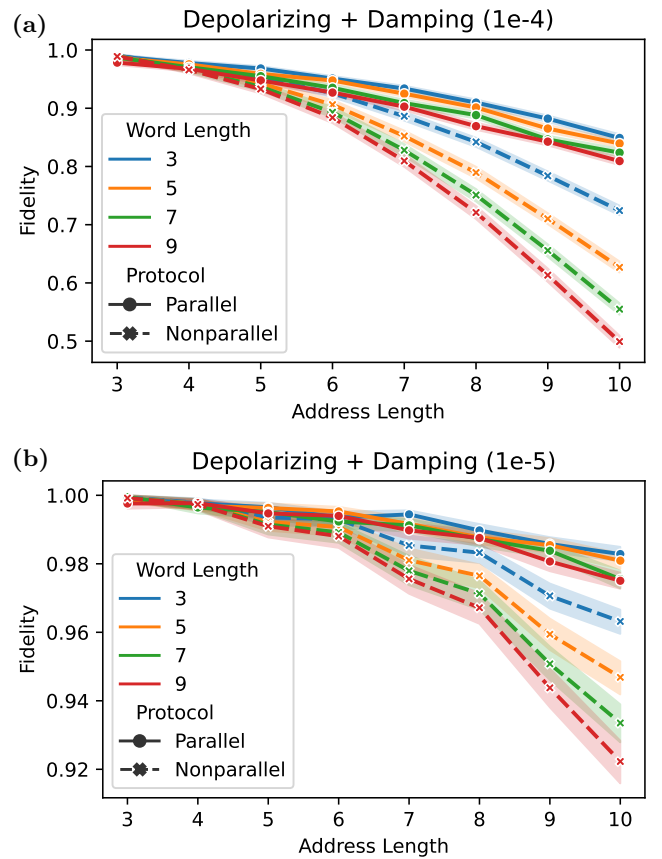


FIG. 5: Results of the classical simulation of QRAM, showing the relation between the fidelity and the address length. (a) Each work qubit/qutrit has $1e-4$ damping and depolarizing noise. Two methods are compared: parallelized (solid lines) and non-parallelized method (dotted lines) when retrieving data with different word lengths. Comparing the dotted line with the solid of the same word length, a substantial fidelity improvement of the parallel protocol can be revealed. (b) Same as (a), but with $1e-5$ damping and depolarizing noise.

this work does not explicitly present the error scaling, we would not compare it directly with our protocols. However, as this method is likely to apply k qubits to independently query each bit of the data, this method is similar to the high-bandwidth protocol with bandwidth k , where the error rate would be at least $O(n^2k)$.

IV. NUMERICAL RESULTS

In this section, we study the fidelity of the parallel protocol with different address sizes and word lengths by a classical simulator and compare it with the nonparallel protocol. The simulation method mainly follows [21] we extend it to simulate the QRAM with arbitrary word length.

The simulation starts from randomly generated QRAM memory and d superposition bus input, that is

$$\sum_i \alpha_i |a_i\rangle |d_i\rangle. \quad (4)$$

During the execution of the QRAM circuit, we apply the damping and/or depolarizing error channels to each working qudit. After the process finishes, the bus will be entangled with the QRAM system. Then we partial-trace the QRAM system and obtain a mixed state in the bus, that is

$$\sum_j p_j |\psi_j\rangle \langle \psi_j|. \quad (5)$$

Finally, we calculate the fidelity F of the output where

$$F = \sum_j p_j |\alpha_i|^2 |\langle a_i, d_i \oplus m_{a_i} | \psi_j \rangle|^2. \quad (6)$$

The above process is repeated 10^4 times to obtain the average fidelity and the standard error.

We compare the parallel and nonparallel protocol for the same (n, k) -QRAM. As the above text has stated, these two protocols have the same structure but different execution processes. In Fig. 5, we plot the change of fidelity with different word lengths. The solid lines and the dotted lines with the same color represent the same error and size configuration with parallel and nonparallel protocol, correspondingly. Both figures with 10^{-4} and 10^{-5} error strength observe that the parallel protocol has substantial improvement in fidelity compared to the nonparallel protocol.

We also conducted simulations to compare the performance of various error channels, and the results are presented in Appendix Section B. Our findings suggest a small difference in the relation between address size n and word length k . However, in all cases, it was observed that the fidelity is affected much weaker by k than by n in the parallel protocol.

V. APPLICATION TO ARBITRARY-SIZED DATA LOADING

The parallel protocol can also be applied to arbitrary-sized data-loading tasks. Firstly, we present the definition here.

Definition 2 (Arbitrary-sized data loading). *A (n, m, k) -data loading task is to load 2^{m+n} -sized of k -bit data with at most n -level QRAM.*

In previous works, this task is accomplished by a hybrid architecture that combines QRAM and QROM. A QROM is a quantum circuit embedding data loader which uses 2^n circuit depth and n qubit. When the address length is $m + n$, we sequentially set the higher digit from 0 to $2^m - 1$ with the QROM, and query the lower

n digit with the QRAM. As the result, the hybrid architecture uses $2^m(n + k)$ time to finish the (n, m, k) -dataset loading when using the parallel QRAM protocol. As the hybrid architecture consists of 2^m sequential and independent QRAM queries, the error scaling is thus $O(2^m(n + k)n^2\epsilon)$ (here we only concentrate on the qutrit-based scheme). Structurally, the hybrid architecture is like the nonparallel protocol which accesses each subset of data sequentially. Inspired by the parallel protocol, we can design a parallel version of the hybrid architecture, which is called the *hybrid-parallel* protocol. The performance is as follows.

Proposition 3 (Performance of the hybrid-parallel protocol on (n, m, k) -dataset loading). *The time complexity of the hybrid-parallel protocol with (n, k) -QRAM on (n, m, k) -data loading task is $2^m k + n$. The error scaling is $O((2^m k + n)n\epsilon) \sim O(2^m nk)$.*

The quantum circuit is shown in Fig. 6, where the i, j are the address bus, *Tree* is the QRAM system, and the *Data Bus* is the data bus. Define i and j are the higher and lower digit of the address register, the task can be written as

$$\sum_{i=0, j=0}^{2^m-1, 2^n-1} \alpha_{i,j} |i\rangle |j\rangle |z\rangle \rightarrow \sum_{i=0, j=0}^{2^m-1, 2^n-1} \alpha_{i,j} |i\rangle |j\rangle |z \oplus d_{i,j}\rangle. \quad (7)$$

The first step is to perform the address setting stage, using $|j\rangle$ to initialize the QRAM tree. Then we modify the data fetch stage from a SWAP to a control-SWAP so that the *data bus input* operation is controlled by the state of the higher digit. The first series load the k -bit when $i = 0$, resulting in

$$\sum_{j=0}^{2^n-1} \alpha_{0,j} |0\rangle |j\rangle |z\rangle \rightarrow \sum_{j=0}^{2^n-1} \alpha_{0,j} |0\rangle |j\rangle |z \oplus d_{0,j}\rangle. \quad (8)$$

And the next series load the k -bit when $i = 1$, etc. After iterating over all 2^m higher digits, we perform the uncomputing to recover the QRAM system.

The time for loading 2^m data is independent with n so that the time complexity is thus $2^m k + n$. Similar to above, the error scaling is $O((2^m k + n)n\epsilon) \sim O(2^m nk)$. Compared with the hybrid architecture, this hybrid-parallel protocol significantly reduces the time and error.

Moreover, we also want to discuss the parallel protocol's ability for loading sparse data. The hybrid-parallel protocol treats the data as 2^n number of dense binary strings where each is of $2^m k$ -sized. This also can be applied to the case when the data is sparsely encoded, where we only have to adjust $2^m k$ to some k' and treat the original data loading task into the (n, k') -QRAM task. For example, a hash table is an array of buckets where each bucket may contain at most M elements. The parallel protocol can use a n -level QRAM and $O(n + Mk)$ time to access all data and error scaling $O((n^2 + nMk)\epsilon)$.

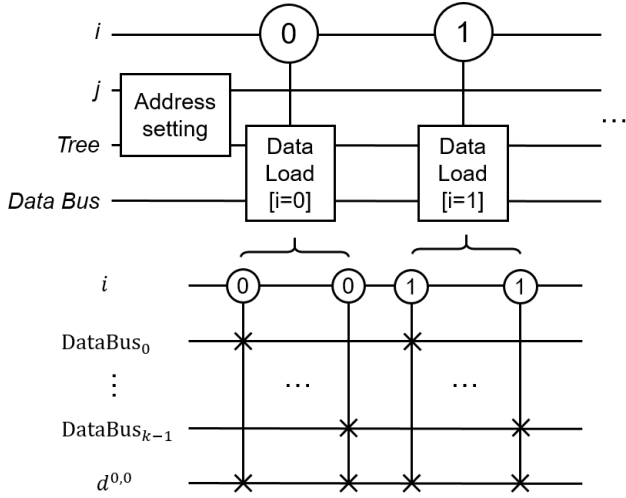


FIG. 6: The quantum circuit for the hybrid-parallel protocol. The above circuit shows the control sequence, where we first perform the address setting stage according to the register j , then we perform the data fetch sequence with each i as the controller. The detail for each data load module is shown at the bottom, where each data bus input is now controlled by register i . After completing all data from $i = 0$, we then load from $i = 1$ and restart from the first digit of the data bus.

VI. SUMMARY AND OUTLOOK

In summary, we propose an optimized protocol which is named *parallel protocol*. The parallel protocol implements (n, k) -QRAM with $O(2^n)$ qubits or qutrits, $O(n + k)$ execution time complexity, and $O((n + k)n\epsilon)$ error rate. Other two possible protocols, the nonparallel protocol, and the high-bandwidth protocol are compared with the parallel protocol, where the time complexity and the number of qubits and qutrits of the parallel protocol have great advantages over its counterparts. More importantly, the error scaling is substantially improved from $O(n^2 k \epsilon)$ to $O((n + k)n\epsilon)$. For large k such as $n \sim k$, the protocol effectively improves the error from $O(n^3)$ to $O(n^2)$. Numerical simulations are performed and demonstrate the improvement of the error performance of the parallel protocol.

The application to the arbitrary-sized data loading task is also discussed. When the number of data entries is 2^{m+n} where only n -level QRAM is given, multiple accesses of QRAM are required. We propose the hybrid-parallel protocol, loading the QRAM with $O(2^m k + n)$ time and $O((2^m k + n)n\epsilon)$ error scaling. This is also a significant improvement over the hybrid architecture that combines the QRAM and QROM.

As the classical data loading task is essential for almost all quantum algorithms that require a large amount of real-world data, we should keep improving the performance of the QRAM. Even the best way for loading more

data bits into the quantum computer is to build a QRAM that can retrieve every data bit in parallel, however, it is always difficult to build a QRAM as large and high-fidelity as we want. Our protocol demonstrates how to apply a small QRAM for big data with better performance than simply querying them sequentially.

ACKNOWLEDGMENTS

This work was supported by the National Natural Science Foundation of China (Grant No. 12034018), and Innovation Program for Quantum Science and Technology No. 2021ZD0302300.

Appendix A: Proof of Error scaling

1. A review of proof for error-resilience of bucket-brigade QRAM

To begin with, we review the idea of proof for noise-resilience of the QRAM in [21]. First, we classify all branches into good branches and bad branches for a certain error configuration c , which represents a configuration of Kraus operators on all qudits and all time steps. A good branch means that the state of all qudits that are related to the corresponding address remains unchanged after applications of Kraus operators. The overlap between good branches and the ideal final state satisfies

$$\langle \psi_{\text{out}} | \text{good}(c) \rangle = \Lambda(c), \quad (\text{A1})$$

where $\Lambda(c)$ is the sum of the amplitude of good branches $\Lambda(c) = \sum_{i \in \text{good}} |\alpha_i|^2$. The fidelity of error configuration c satisfies $F(c) \geq (2\Lambda(c) - 1)^2$ for $\Lambda(c) > 1/2$.

The fidelity is the average of $F(c)$ for all possible error configurations, that is

$$F = \mathbb{E}(F(c)) \geq \mathbb{E}(2\Lambda(c) - 1)^2 \geq (2\mathbb{E}(\Lambda) - 1)^2. \quad (\text{A2})$$

Here $\mathbb{E}(\Lambda)$ is the average fraction of good branches, which is computed iteratively and finally yields $\mathbb{E}(\Lambda) = (1 - \epsilon)^{T \log N} \geq 1 - \epsilon T \log N$. Combining this inequality with Eqn. A2, we obtain the final result

$$F \geq 1 - 4\epsilon T \log N = 1 - 4\epsilon n T. \quad (\text{A3})$$

For the qubit-based scheme, most of the processes preserve the same, except $\mathbb{E}(\Lambda)_b = (1 - \epsilon)^{T n^2} \geq 1 - \epsilon T n^2$.

2. Error scalings for three protocols

In the main text, we stated that the error scaling of each protocol can be obtained by replacing the time complexity T and the error of each qubit ϵ with corresponding values. To show this can be directly used to extend

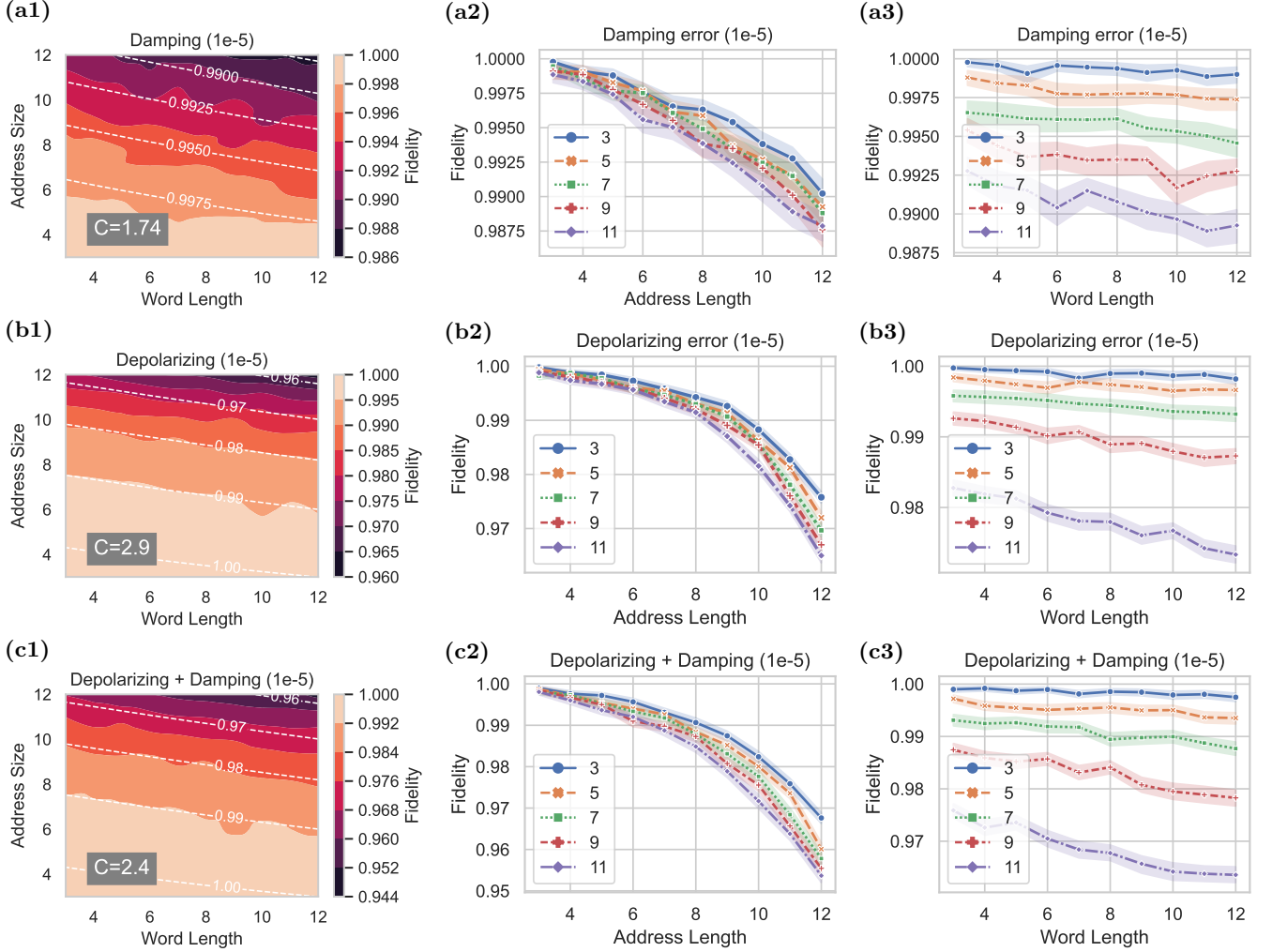


FIG. 7: Fidelity for various error channel types. (a1-a3) Only a damping channel is applied. (b1-b3) Only a depolarizing channel is applied. (c1-c3) Both a damping and a depolarizing channel are applied. (a1-c1) Heatmaps illustrating the relationship between fidelity, address size n , and word length k for different error channels. The contour line depicts the relation between n and k based on the fitting formula. (a2-c2) Fidelity as a function of address size, with each line corresponding to a different word length as shown in the legend. (a3-c3) Fidelity as a function of word length, with each line corresponding to a different address size as shown in the legend.

the proof for the parallel protocol, we should also show that the “good branch” has the same definition in these protocols.

First, the error in the bad branch will not be propagated to any good branch. At the data fetch stage, the data bits are only transferred through the data qubit in the node. When there is no error on the address qubit, a bad branch cannot pass the error to the good branch the same as how the normal bucket-brigade architecture does. Second, the fraction of the good branch is $1 - O(nT\epsilon)$. Because $T\epsilon$ is the total error for a qubit that undergoes T time steps, we only have to change T to the number of time steps in the parallel protocol.

For the nonparallel protocol, it repeats the data fetch stage k times. Note that the data fetch stage still has $O(n^2\epsilon)$ error scaling even if there is no error in the address

setting and uncomputing stage, which has been proved in [21]. Therefore, the error scaling for the nonparallel protocol is at least $O(kn^2\epsilon)$ when k scales.

The high-bandwidth protocol has the same structure and process as the original bucket-brigade QRAM. We can bind all data qubits in a node as a quasiparticle with 2^k levels. When each qubit has an error rate ϵ , this quasiparticle’s fidelity is $(1 - \epsilon)^k \sim 1 - k\epsilon$. Therefore, we only have to replace ϵ with $k\epsilon$ in the error scaling expression.

Appendix B: The scaling of QRAM fidelity through numerical experiments

We test the change of QRAM fidelity with a certain error channel with the address size and word length, whose results are illustrated in Fig. 7. The error channel is the

damping channel where $\gamma = 10^{-5}$ (details about damping channel) in subfigure (a) series, the depolarizing channel where $p = 10^{-5}$ in subfigure (b) series, and the compound of the above two channels in subfigure (c) series. Both the address size n and word length k range from 3 to 12, and the contour map is plotted in Fig. 7(a1), (b1) and (c1). The contour line is fitted from the following formula:

$$F = 1 - A(Cn^2 + nk)\epsilon. \quad (\text{B1})$$

The variable C represents the relative magnification of the variable affected by the two dominated terms n^2 and nk , where fitting results show the correct relation on F with n and k . In Fig. 7(a2), (b2) and (c2), different lines represent the corresponding word lengths; in Fig. 7(a3), (b3) and (c3), different lines represent the corresponding address sizes. These figures imply a mild and linear dependency of the fidelity on the word length, and the increasing n will induce a quadratic increase in the error rate.

-
- [1] F. Arute, K. Arya, R. Babbush, D. Bacon, J. C. Bardin, R. Barends, R. Biswas, S. Boixo, F. Brandao, D. A. Buell, B. Burkett, Y. Chen, Z. Chen, B. Chiaro, R. Collins, W. Courtney, A. Dunsworth, E. Farhi, B. Foxen, A. Fowler, C. Gidney, M. Giustina, R. Graff, K. Guerin, S. Habegger, M. P. Harrigan, M. J. Hartmann, A. Ho, M. Hoffmann, T. Huang, T. S. Humble, S. V. Isakov, E. Jeffrey, Z. Jiang, D. Kafri, K. Kechedzhi, J. Kelly, P. V. Klimov, S. Knysh, A. Korotkov, F. Kostitsa, D. Landhuis, M. Lindmark, E. Lucero, D. Lyakh, S. Mandra, J. R. McClean, M. McEwen, A. Megrant, X. Mi, K. Michielsen, M. Mohseni, J. Mutus, O. Naaman, M. Neeley, C. Neill, M. Y. Niu, E. Ostby, A. Petukhov, J. C. Platt, C. Quintana, E. G. Rieffel, P. Roushan, N. C. Rubin, D. Sank, K. J. Satzinger, V. Smelyanskiy, K. J. Sung, M. D. Trevithick, A. Vainsencher, B. Villalonga, T. White, Z. J. Yao, P. Yeh, A. Zalcman, H. Neven, and J. M. Martinis, Quantum supremacy using a programmable superconducting processor, *Nature* **574**, 505 (2019).
 - [2] Y. Wu, W.-S. Bao, S. Cao, F. Chen, M.-C. Chen, X. Chen, T.-H. Chung, H. Deng, Y. Du, D. Fan, M. Gong, C. Guo, C. Guo, S. Guo, L. Han, L. Hong, H.-L. Huang, Y.-H. Huo, L. Li, N. Li, S. Li, Y. Li, F. Liang, C. Lin, J. Lin, H. Qian, D. Qiao, H. Rong, H. Su, L. Sun, L. Wang, S. Wang, D. Wu, Y. Xu, K. Yan, W. Yang, Y. Yang, Y. Ye, J. Yin, C. Ying, J. Yu, C. Zha, C. Zhang, H. Zhang, K. Zhang, Y. Zhang, H. Zhao, Y. Zhao, L. Zhou, Q. Zhu, C.-Y. Lu, C.-Z. Peng, X. Zhu, and J.-W. Pan, Strong quantum computational advantage using a superconducting quantum processor, *Physical Review Letters* **127**, 180501 (2021).
 - [3] M. Ekerå and J. Hastad, Quantum algorithms for computing short discrete logarithms and factoring rsa integers, *Post-Quantum Cryptography, Pqcrypto 2017* **10346**, 347 (2017).
 - [4] H.-Y. Huang, M. Broughton, M. Mohseni, R. Babbush, S. Boixo, H. Neven, and J. R. McClean, Power of data in quantum machine learning, *Nature communications* **12**, 2631 (2021).
 - [5] J. Biamonte, P. Wittek, N. Pancotti, P. Rebentrost, N. Wiebe, and S. Lloyd, Quantum machine learning, *Nature* **549**, 195 (2017).
 - [6] I. Kerenidis, J. Landman, and A. Prakash, Quantum algorithms for deep convolutional neural networks, in *International Conference on Learning Representations* (2020).
 - [7] B. T. Kiani, G. De Palma, D. Englund, W. Kaminsky, M. Marvian, and S. Lloyd, Quantum advantage for differential equation analysis, *Physical Review A* **105**, ARTN 022415 10.1103/PhysRevA.105.022415 (2022).
 - [8] C. Xue, Y. C. Wu, and G. P. Guo, Quantum homotopy perturbation method for nonlinear dissipative ordinary differential equations, *New Journal of Physics* **23**, ARTN 123035 10.1088/1367-2630/ac3eff (2021).
 - [9] J. P. Liu, H. O. Kolden, H. K. Krovi, N. F. Loureiro, K. Trivisa, and A. M. Childs, Efficient quantum algorithm for dissipative nonlinear differential equations, *Proceedings of the National Academy of Sciences of the United States of America* **118**, ARTN e2026805118 10.1073/pnas.2026805118 (2021).
 - [10] Z. Y. Chen, C. Xue, S. M. Chen, B. H. Lu, Y. C. Wu, J. C. Ding, S. H. Huang, and G. P. Guo, Quantum approach to accelerate finite volume method on steady computational fluid dynamics problems, *Quantum Information Processing* **21**, ARTN 137 10.1007/s11128-022-03478-w (2022).
 - [11] M. Cerezo, G. Verdon, H.-Y. Huang, L. Cincio, and P. J. Coles, Challenges and opportunities in quantum machine learning, *Nature Computational Science* **2**, 567 (2022).
 - [12] C. Ciliberto, M. Herbster, A. D. Ialongo, M. Pontil, A. Rocchetto, S. Severini, and L. Wossnig, Quantum machine learning: a classical perspective, *Proceedings of the Royal Society A: Mathematical, Physical and Engineering Sciences* **474**, 20170551 (2018).
 - [13] S. Aaronson, Read the fine print, *Nature Physics* **11**, 291 (2015).
 - [14] V. Giovannetti, S. Lloyd, and L. Maccone, Quantum random access memory, *Physical Review Letters* **100**, ARTN 160501 10.1103/PhysRevLett.100.160501 (2008).
 - [15] V. Giovannetti, S. Lloyd, and L. Maccone, Architectures for a quantum random access memory, *Physical Review A* **78**, ARTN 052310 10.1103/PhysRevA.78.052310 (2008).
 - [16] K. C. Chen, W. H. Dai, C. Errando-Herranz, S. Lloyd, and D. Englund, Heralded quantum random access memory in a scalable photonic integrated circuit platform, *2021 Conference on Lasers and Electro-Optics (CLEO)* (2021).
 - [17] R. Asaka, K. Sakai, and R. Yahagi, Two-level quantum walkers on directed graphs. ii. application to quantum random access memory, *Physical Review A* **107**, 022416 (2023).
 - [18] R. Asaka, K. Sakai, and R. Yahagi, Quantum random access memory via quantum walk, *Quantum Science and Technology* **6**, ARTN 035004 10.1088/2058-9565/abf484 (2021).

- [19] K. R. Patton and U. R. Fischer, Ultrafast quantum random access memory utilizing single rydberg atoms in a bose-einstein condensate, *Physical Review Letters* **111**, ARTN 240504 10.1103/PhysRevLett.111.240504 (2013).
- [20] S. A. Moiseev and S. N. Andrianov, Photon echo quantum random access memory integration in a quantum computer, *Journal of Physics B-Atomic Molecular and Optical Physics* **45**, ArtN 124017 10.1088/0953-4075/45/12/124017 (2012).
- [21] C. T. Hann, G. Lee, S. M. Girvin, and L. Jiang, Resilience of quantum random access memory to generic noise, *Prx Quantum* **2**, ARTN 020311 10.1103/PRXQuantum.2.020311 (2021).
- [22] M. Newman and Y. Shi, Limitations on transversal computation through quantum homomorphic encryption, *arXiv preprint arXiv:1704.07798* (2017).
- [23] B. Zeng, A. Cross, and I. L. Chuang, Transversality versus universality for additive quantum codes, *IEEE Transactions on Information Theory* **57**, 6272 (2011).
- [24] B. Eastin and E. Knill, Restrictions on transversal encoded quantum gate sets, *Physical review letters* **102**, 110502 (2009).
- [25] A. G. Fowler, M. Mariantoni, J. M. Martinis, and A. N. Cleland, Surface codes: Towards practical large-scale quantum computation, *Physical Review A* **86**, 032324 (2012).
- [26] G. Lee, C. T. Hann, S. Puri, S. Girvin, and L. Jiang, Error suppression for arbitrary-size black box quantum operations, *arXiv preprint arXiv:2210.10733* (2022).
- [27] J. M. Martyn, Z. M. Rossi, A. K. Tan, and I. L. Chuang, Grand unification of quantum algorithms, *PRX Quantum* **2**, 040203 (2021).
- [28] A. M. Childs, R. Kothari, and R. D. Somma, Quantum algorithm for systems of linear equations with exponentially improved dependence on precision, *SIAM Journal on Computing* **46**, 1920 (2017).